Electrochimica Acta 446 (2023) 142104

Contents lists available at ScienceDirect

Electrochimica Acta

journal homepage: www.journals.elsevier.com/electrochimica-acta

Brewery waste derived activated carbon for high performance electrochemical capacitors and lithium-ion capacitors

Sandesh Darlami Magar [a], Christian Leibing [a], Juan Luis Gómez-Urbano [b], Rosalía Cid [b], Daniel Carriazo [b,c], Andrea Balducci [a,*]

[a] Institute for Technical Chemistry and Environmental Chemistry and Center for Energy and Environmental Chemistry Jena (CEEC Jena) Philosophenweg 7a, Friedrich Schiller University Jena, Jena 07743, Germany

[b] Basque Research and Technology Alliance (BRTA) Alava Technology Park, Centre for Cooperative Research on Alternative Energies (CIC energiGUNE), Albert Einstein 48, Vitoria-Gasteiz 01510, Spain

[c] IKERBASQUE, Basque Foundation for Science, Bilbao 48013, Spain

ARTICLE INFO

Keywords:
Brewery waste
Hard carbon
Activated carbon
Electric double layer capacitor
Lithium-ion capacitor

ABSTRACT

In this study we report about the synthesis and characterization of an activated carbon (AC) displaying very large surface area (~3600 m^2 g^{-1}) obtained from a cheap and abundant brewery waste product (Brewer's spent grains, BSG). AC based electrodes prepared from BSG demonstrated a very high specific capacitance (46 F g^{-1}) and capacitance retention when evaluated in symmetric Electrical Double Layer Capacitors (EDLCs) devices with organic electrolytes. We showed that these electrodes can be successfully utilized for the realization of lab scale EDLCs and Lithium-ion Capacitors exhibiting very high energy and power densities as well excellent cycling stability (85% capacitance retention after 200 h of float test). Considering these results, the BSG-derived AC can be certainly considered as very promising material, which can contribute to the development of high performance, cost effective and eco-friendly high-power devices.

1. Introduction

The Electric double layer capacitor (EDLCs) are currently considered as one of the most important energy storage devices in our society owing to their high-power capabilities (>10 kW/kg), fast response time (<1 min) and longevity (>1 million cycles)[1]. These systems are already used in a wide span of applications including energy and utilities, consumer electronics, aerospace, military, industrial and medical fields [2,3]. However, their low energy density (<10 Wh kg^{-1}) and fast self-discharge rate remain a major challenge, which is limiting their use in several applications, particularly in transportation sector. For this reason, great efforts are presently directed toward the realization of high energy EDLCs. To reach this goal, the development of cheap materials displaying high capacitance is essential.

Carbonaceous materials are since long time considered as one of the most suitable electrode materials for EDLCs and, more in general, for energy storage devices. This is mainly due to the fact that, there is a possibility to realize a large variety of different materials, e.g. carbon sphere [4], carbon nanotubes [5,6], graphene [7,8], carbon black [9], carbon fibres [10], carbon aerogels [11], carbide derived carbon [12], templated carbon [13,14] and activated carbons that display interesting properties for energy storage application.

Activated carbons (AC) display high surface area (>1000 m^2 g^{-1}), high electronic conductivity, good chemical stability, and low cost of production. These properties make them very well-suited materials for the realization of energy storage devices relying in physical storage (formation/depletion of electric double layer) at electrode-electrolyte interface such as EDLCs. In the last years a large number of different ACs have been proposed and investigated, and it has been shown that the pore structures of these materials are strongly influencing the electrochemical performance. The realization of hierarchical structures interconnected with micro and mesopores appears necessary to maximize the amount charge stored and its deliver and uptake [15–18].

A very important aspects while considering AC is their production process, and especially the precursor materials that are used to synthesize them. As a matter of fact, the use of largely available, cheap, and eco-friendly precursor is indispensable to realize AC that can be produced in large scale and with prices that are acceptable for the realization of commercial EDLCs. In this regard, biomass is nowadays considered as one of the most promising precursors of AC as its use allow

* Corresponding author.
E-mail address: andrea.balducci@uni-jena.de (A. Balducci).

https://doi.org/10.1016/j.electacta.2023.142104
Received 12 December 2022; Received in revised form 25 January 2023; Accepted 21 February 2023
Available online 24 February 2023

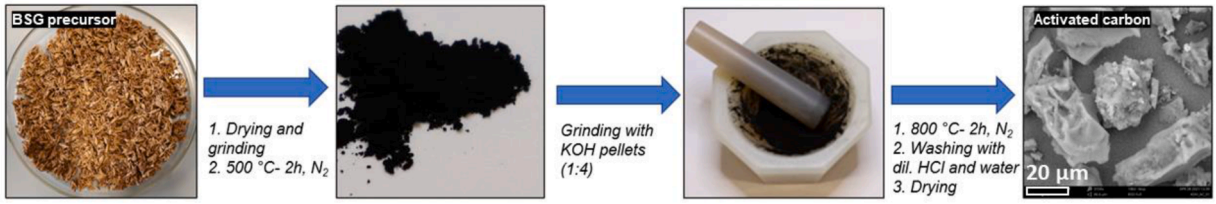

Fig. 1. Schematic diagram of Activated carbon synthesis from Brewer's spent grains precursor.

the realization of AC displaying tuneable properties and able to display high electrochemical performance when used in EDLCs [19,20]. Example of biomasses utilized to synthesized AC suitable for EDLCs are rice husks [21], dragon fruit peels [22], coffee waste [23,24], wine waste [25], coconut shells [26] etc.

In a recent work, we showed that brewer's spent grain (BSG), which is a largely available, easy to process, and logistically advantageous agro-industrial bio-waste, can be conveniently utilized for the realization of hard carbon (HC) electrodes [27]. BSG is a major waste (represent about 85% of total by-products) on the beer production process, and Germany alone produce approximatively 1.5 billion tons of wet BSG per year [28]. It is primarily composed of cellulose, hemicellulose, lignin and non-lignocellulose components such as starch, proteins, ash etc. showing rich textural, chemical and elemental composition and, therefore has been considered as an interesting precursor material of AC[29, 30]. To the best of our knowledge, however, this latter use has not been considered so far.

In this study we report about the synthesis and characterization of AC realized from BSG. These ACs have been utilized for the realization of EDLCs and, also for lithium-ion capacitors (LICs). In these latter devices, these electrodes have been used in combination with HC synthesized from BSG.

2. Experimental

2.1. Materials

Brewer's spent grains was collected from Jena brewery (Papiermühle) in Germany. The sample was immediately dried at 80 °C for 48 h to avoid microbial growth. The dried sample was grounded into sizes widely ranging between 0.2–4 mm by using mortar and pestle. The estimated composition of the sample after Thermogravimetric analysis (TGA) showed a lignin content between 35-45%, cellulose and hemicellulose of 40–50% and 5% of ash content [27].

3. Methods

The grounded BSG sample was pre-carbonized at 500 °C for 2 h under nitrogen flow at 110 ml/min and a ramp rate of 5 °C/min to obtain a char. For the activation, the char was first impregnated with potassium hydroxide (KOH) pellets at two different ratios of 1:2 and 1:4 using mortar and pestle. Then the impregnated char mixtures were heated inside a tubular furnace (ThermConcept) at 800 °C for 2 h under nitrogen flow at 110 ml/min and a ramp rate of 5 °C/min. The resulting samples after activation were treated with dil. HCl and distilled water to recover the carbon. Finally, the carbon was dried at 80 °C for 24 h before further analysis. Fig. 1 is reporting the schematic diagram of activated carbon synthesis steps from BSG precursor at impregnation ratio of 1:4. The carbon yield at two different impregnation ratios of 1:2 and 1:4 is 10% and 6.4% respectively.

3.1. Material characterization

The surface topography of the carbon was obtained from scanning electron microscope (SEM) (Quanta200 FEI) at 3 kV, 15 kV and 30 kV. X-ray Photoelectron Spectroscopy (XPS) was conducted to evaluate the elemental and chemical composition of the carbon surface using a Phoibos 150 spectrometer (SPECS Surface Nano Analysis) in Fixed Analyzer Transmission mode and a non-chromatic Mg X-ray source (Kα with hν=1253.6 eV). CasaXPS software was used to treat the experiment data. The background of inelastically scattered photoelectrons was simulated by a Shirley function and a Voigt profile (30% Gaussian, 70% Lorentzian) was employed as line-shape for all components except for semi-metallic sp^2 C = C. Aromatic carbon asymmetry was defined as in the Doniach-Sunjic (DS) model [31], but using an asymmetric pseudo-Voigt (APV) function instead to overcome the integral divergence of the DS function. The specific surface areas (SSA), pore volume and pore size distribution of carbonaceous materials were estimated by analyzing N_2 sorption isotherms (at 77.3 K), measured by an Autosorb iQ3 machine from Quantachrome Corporation. The total surface area is calculated using multiple point Brunauer, Emmett and Teller (BET) method in the partial pressure range between 0.05–0.30. The pore size distribution was determined by applying quenched solid density functional theory (QSDFT). Raman spectra were measured with an InVia confocal Raman microscope from Renishaw with excitation at wavelength of 532 nm. The Raman intensity ratio (I_D/I_G) of carbon sample was calculated from the deconvoluted peaks of D and G-band using Lorentzian fit (OriginPro software). X-ray diffraction pattern was measured using X-ray diffractometer (Bruker D8). The data were collected using CuKα radiation over 2θ within the range from 10 to 80 at steps of 0.02.

3.2. Electrode fabrication and electrochemical testing

The activated carbon electrodes were prepared by casting a slurry containing the synthesized activated carbon, conducting carbon (Super C60, Imerys) and carboxymethyl cellulose (Walocel CRT 2000 PA, Brenntag) dissolved in water (with a weight ratio 90:5:5), upon KOH etched aluminium foil. The casting was dried at room temperature and afterwards punched into 12 mm diameter shaped disc electrodes. The mass loading of the electrodes was in between the range of 1–1.8 mg cm^{-2}. Vacuum drying of electrodes at 80 °C for 24 h was performed before transferring inside argon glove box. EDLCs were assembled by utilizing two identical AC electrodes separated by a glass microfiber filter (Whatman) soaked with 150 µl of 1 M Triethylmethylammonium Tetrafluoroborate ($TEMABF_4$) dissolved in acetonitrile (Skeleton technology) and inside a Swagelok type cells.

Hard carbon (HC) based electrodes were also prepared by casting slurry mixture of hard carbon sample obtained from BSG [27], conducting carbon and carboxymethyl cellulose dissolved in water (90:5:5, mass ratio) upon a copper foil. HC based electrodes were evaluated in three electrodes cell setup against lithium metal (counter and reference electrodes) at potential range between 0.005–2 V vs. Li^+/Li using 1 M lithium hexafluorophosphate ($LiPF_6$) dissolved in ethylene carbonate and dimethyl carbonate (1:1 wt ratio) as electrolyte (LP30, Solvionic).

LICs were assembled by coupling HC electrode and AC electrode in three cell setups against lithium metal as reference electrode. The HC electrode was pre-lithiated by assembling half-cell against lithium metal and charging to 5 mV vs. Li^+/Li and the AC electrode was pre-cycled at potential range between 2.0–4.3 V vs. Li^+/Li then the electrodes were

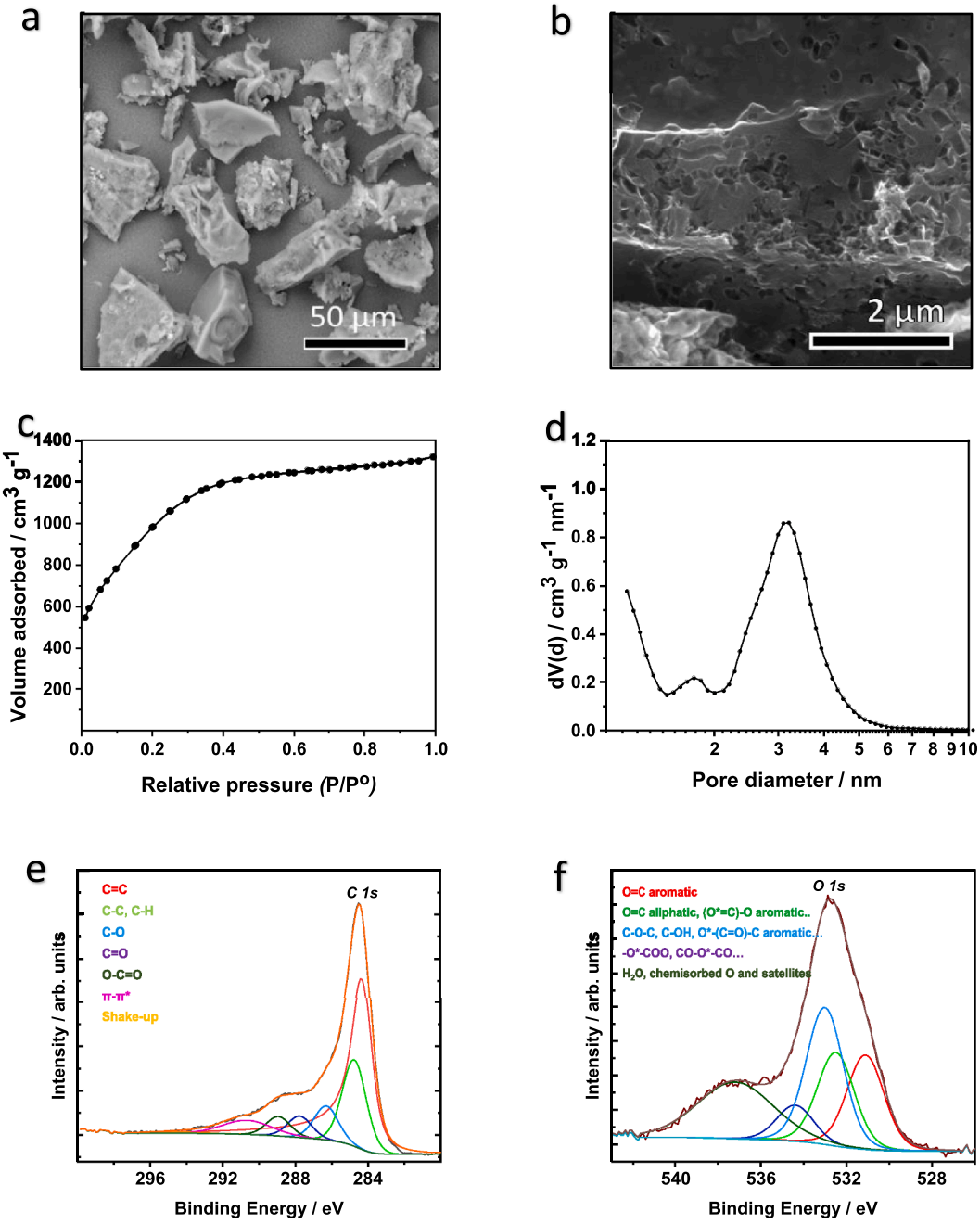

Fig. 2. (a), (b) SEM images of activated carbon (c) Nitrogen physisorption isotherm (d) pore size distributions of activated carbon, (e) C1s and f) O1s deconvoluted XPS spectrum of activated carbon sample.

Table 1
Properties of BSG derived activated carbon.

Sample	S_{BET} /m^2 g^{-1}	Pore volume /cm^3 g^{-1}	Mean pore diameter /nm	Raman intensity ratio	Surface elemental composition (XPS)
AC	~3600	1.8	3.2	2.3	Oxygen 23.4%, Carbon 76.6%

recovered by disassembling the cell. The mass ratio of the two electrodes were fixed at 1:1. The LICs were cycled between 2.0–4.3 V vs. Li^+/Li in LP30.

Galvanostatic Charge-Discharge (GCD) at different current rates of 0.5, 1, 2, 5, 10, 20 A g^{-1} and Cycling Voltammetry (CV) measurements at scan rate of 5, 10, 20, 50, 100, 200 mV s^{-1} of symmetric EDLCs were performed in VMP-3 (BioLogic) potentiostat. The stability of the EDLC was evaluated by holding cell voltage at 2.7 V for 200 h. GCD cycles at 1 A g^{-1} were carried out every 10 h to monitor the changes in capacitance. The electrochemical impedance spectroscopy of the device was measured at fully discharged state from 100 mHz to 1 MHz in VMP-3 (BioLogic) at room temperature. The GCD of half-cells containing hard carbon electrode against lithium metal were performed in Arbin Instruments (LBT21084) at current densities ranging from 0.1 C to 10 C (1C = 0.372 A g^{-1}) between 5 mV–2 V vs. Li^+/Li. The LICs were cycled utilizing VMP-3 (BioLogic) at current densities of 0.1, 0.5, 1, 2 and 5 A g^{-1} between 2.0–4.3 V vs. Li^+/Li. The cyclability of the device is evaluated by performing long term GCD at current density of 1 A g^{-1}.

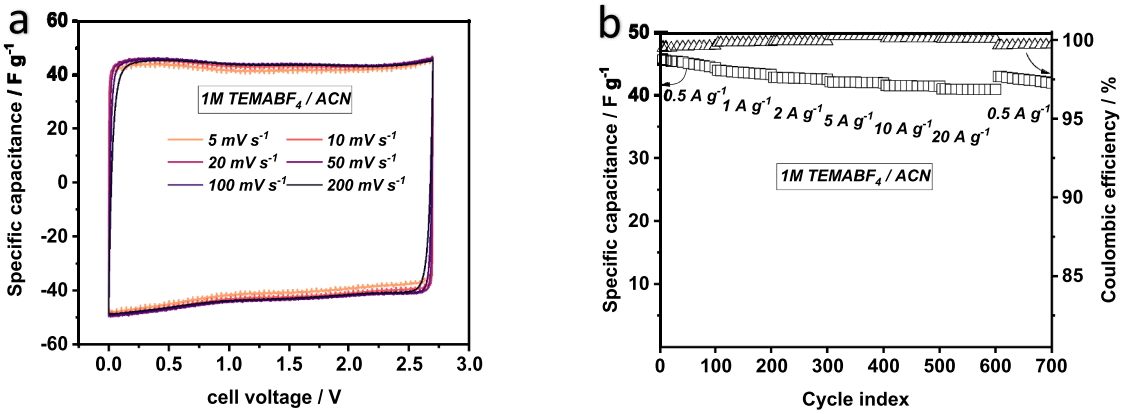

Fig. 3. (a) Cyclic Voltammogram and (b) rate performance of activated carbon (calculated from GCD) in $TEMABF_4$ /ACN (full cell measurements) between 0–2.7 V.

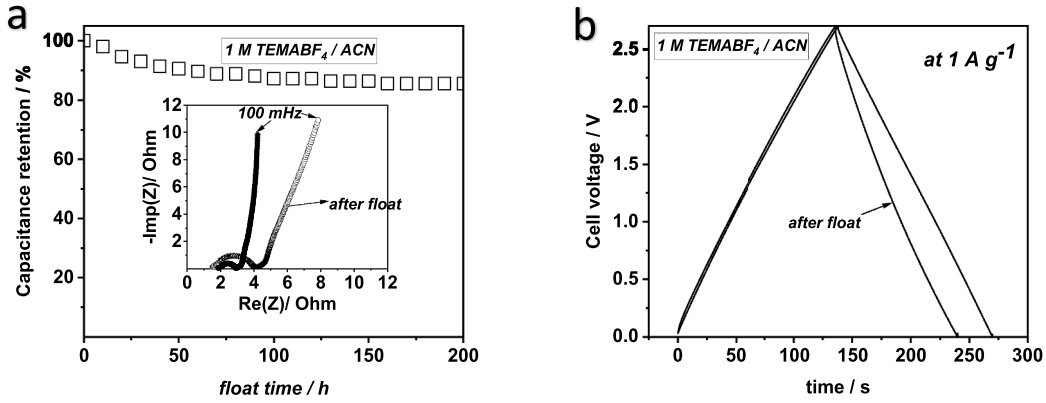

Fig. 4. (a) Capacitance retention during float test at 2.7 V with Nyquist plot and (b) Galvanostatic Charge/Discharge curve of EDLC (before and after float test) in $TEMABF_4$ /CAN (full cell measurements).

The specific capacitance (C_{sp}), Energy density (E_d), Power density (P_d) were calculated using the following equation:

(i) $C_{sp} = \frac{I}{s \times M}$

(ii) $C_{sp} = \frac{I}{dV/dt \times M}$

(iii) $Energy\ density = \frac{I \int V\, dt}{M}$

(iv) $power\ density = \frac{E_d}{t}$

Where, 'I' is a current, 's' is the scan rate, 'M' is the active mass of electrode, 't' is time of discharge and 'V' is the cell potential.

4. Results and discussion

The AC obtained from BSG display irregular, blocky and sheet shapes (Fig. 2a and b). The visible cavities and open channels visible on the images are indicating a retention of the textural properties of the precursor (SEM images of BSG precursor are available in Fig. S 1a and b of Supporting Information (SI)). Fig. 2c and d show nitrogen physisorption isotherms and the pore size distribution of the investigated AC. As shown, the isotherm displays a profile between type I and IV showing a progressive increase on the volume of adsorption, rising to 0.3 value of relative pressure, which indicates the presence of pores that range from small micropores to small mesopores. The BET surface area of the AC was calculated to be ~ 3600 m^2g^{-1} and its pore volume were 1.8 $cm^3 g^{-1}$. It is important to notice that the BET surface area of the AC investigated in this work is larger than that observed for most of biomasses derived AC reported so far in literature [21–26,32,33]. This outcome can be a result of a rich textural property of the BSG precursor, favouring the development of extended pore structures during activation. In addition, the synthesis conditions (activating agent, impregnation ratio, annealing temperature and time) applied in the work have proven to be very effective for obtaining highly porous carbon by many [21,34,35]. Overall, the AC realized from BSG appears as a material with a very high surface area and a large pore volume, that is containing a large amount of meso- and microporous structures.

XPS analysis reveals the AC contains heteroatoms which are mainly based on i.e. C = O carbonyl groups, C—OH/C—O-C (hydroxil, epoxy or ether) groups, and carboxylic (O = C—O-) groups. Fig. 2e, f shows the deconvoluted peaks of C 1 s and O 1 s respectively. The presence of aromatic sp^2 C = C bonds is revealed by the main asymmetric peak at 284.3 eV in the C 1 s spectrum, with related secondary loss peaks at 290.7 eV (π-π* satellites) and 294.4 eV (shake-up). The peak at 284.8 eV corresponds to sp^3 bonded carbons, with some contribution of C = C bonds in the vicinity of oxygen functionalities. While the different oxygen functional groups are relatively well separated in the C 1 s spectrum, their signals strongly overlap in the O 1 s spectrum, making the deconvolution of O 1 s much more complex [36,37]. However, the appearance of the broad and intense peak centered around 537 eV may be partly attributed to the satellites of aromatic oxygen functionalities [38], indicating the oxygen decoration of the aromatic carbon rings (Additionnal XPS data are available in Fig. S3 of SI).

As expected, the Raman spectrum (Fig. S 2a in SI) indicates the non-graphitizable nature of the AC. The AC displays two prominent peaks at 1500 and 1600 cm^{-1} corresponding to defect induced band and graphitic band (Fig. S 2a in SI). The presence of D-band and calculated Raman intensity ratio >1 (see table I) indicates that the sample displays

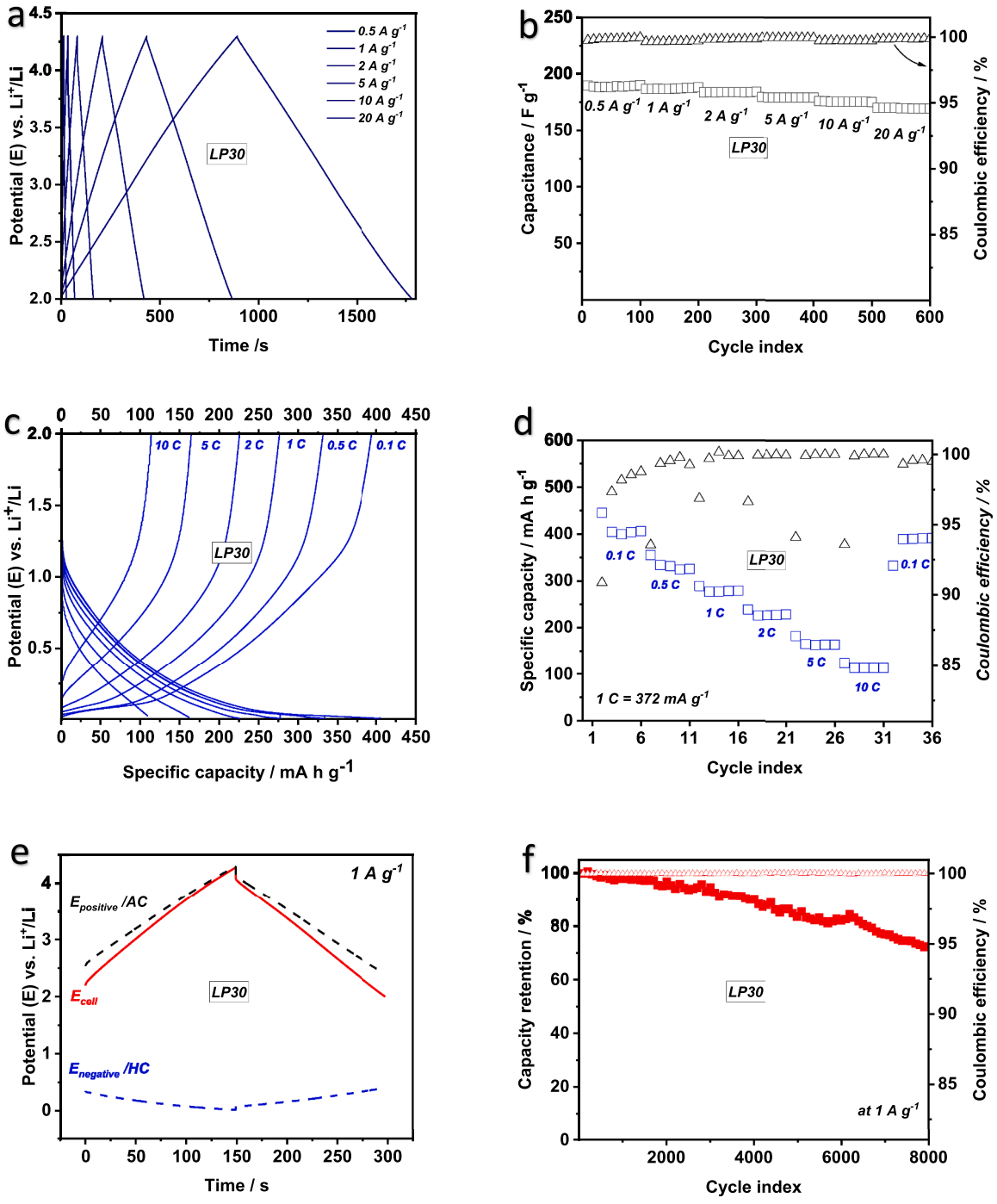

Fig. 5. Galvanostatic charge/discharge curve and rate performance of BSG derived activated carbon in (a), (b) and hard carbon in (c), (d) (half-cell measurements) and (e) (f) displays galvanostatic charge/discharge curve and cycle stability of lithium-ion capacitor during float test, respectively.

significant disorder in the carbon lattice structure [39]. Two broad peaks are observed from XRD measurement at 23° and 43° (see Fig. S 2b in SI), which are assigned to 002 and 100 reflections, suggest the disorder nature for the activated carbon sample. That was also the case for the hard carbon derived from same precursor [27]. Table 1 summarize the main properties of AC obtained from BSG.

4.1. Activated carbon in symmetric EDLC

After the morphological and structural characterization, the BSG-derived AC electrodes have been used for the realization of EDLC containing 1 M $TEMABF_4$ in ACN as electrolyte. Fig. 3a compares the cyclic voltammogram of this device at variable scan rate ranging from 5 mV s^{-1} to 200 mV s^{-1}. It can be observed that the device displays very high specific capacitances regardless the scan rate applied and that the typical rectangular shape of EDLC is even maintained when increasing the scan rate up to 200 mV s^{-1}. As shown in Fig. 3b, when a current density equal to 0.5 A g^{-1} was applied, the device displayed specific capacitance of 46 F g^{-1}. It is important to remark that this value of specific capacitance (which is referred to the mass loading of the two

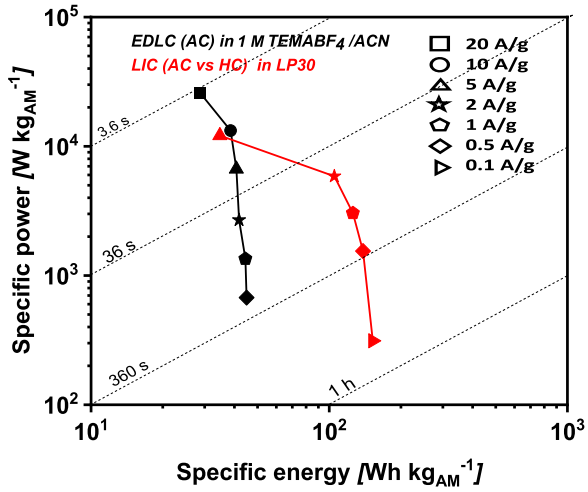

Fig. 6. Ragone plot (comparison of the energy and power densities of EDLC and LIC).

electrodes) is extremely high for an AC electrode and is almost double that of exhibited by analogous lab scale device containing commercial activated carbon (e.g., YP-80 F) and same electrolyte (see Fig. S 6 in SI). Furthermore, it is important to observe that the BSG-derived AC displays outstanding capacitance retention at high current densities. At 10 A g^{-1}, the EDLC retains a capacitance of 41 F g^{-1}, which is 90% of initial capacitance (see Fig S 4 in SI for GCD curve). These capacitance retentions are among the highest reported in literature for AC based EDLCs [21–26,32,33] and it is reasonable to suppose that they are possible due to large availability of accessible micropores and mesoporous structure, which is very favourable for the ion mobility.

With an aim to further investigate the performance of EDLC and its stability, a float test at 2.7 V has been considered. As shown in Fig. 4a, after 200 h of floating at this voltage, the cell was able to retain about 80% of its initial capacitance. As shown in the Nyquist plot (inset of Fig. 4a), during the time of floating the charge transfer resistance within in the device increases. This increase of resistance is leading to a decrease of capacitance and to a less ideal charge/discharge profile, as shown in Fig. 4b. This aging behaviour has been observed for many activated carbon based EDLCs [40–42] tested in comparable conditions and, therefore, is not surprising. Nonetheless, it is worth mentioning that although the device was not optimized, the stability is comparable to that of EDLCs containing AC obtained from other biomasses reported in literature [21–26,32,33] (see SI 12 Table 1). Taking these results into account, the BSG-derived AC can be regarded as a highly promising material for the realization of high performance EDLCs.

4.2. Activated carbon in lithium-ion capacitor (LIC)

In the last years the interest towards lithium-ion capacitor has increased significantly. This interest is motivated by the high energy density that can be delivered by these devices, which can be substantially higher than that of EDLCs. As in the case of EDLCs, also for LIC the possibility to utilized electrodes prepared from cheap and sustainable resources is of great importance. As mentioned in the introduction, in a previous work [27] we investigated the synthesis and use of HC obtained from BSG and we showed that these carbonaceous materials display an excellent electrochemical performance in terms of capacity, capacity retention and stability. Thus, they are interesting candidates for their application as negative electrodes in LIC.

Considering the promising performance of AC and HC obtained from BSG, we therefore decided to realize a LIC containing these electrodes and LP30 as electrolyte. Fig. 5a, shows the charge-discharge profile of the AC based electrode (positive) in LP30 between 2 and 4.3 V vs. Li^+/Li. This voltage range has been selected based upon i) Evaluation of upper potential limit (see Fig. S 7 in SI) and ii) Fixing a lower potential at 2 V vs. Li^+/Li to avoid lithium consumption at positive electrode. As shown, also in this electrolyte the AC electrode displays the typical triangular shape, and no significant faradaic contributions are visible (see Fig. S 8 in SI for CV profile). Furthermore, as it is well visible in Fig. 5b, it displays a very high capacitance (186 F g^{-1} at 1 A g^{-1}) and very high capacitance retention (176 F g^{-1} at 10 A g^{-1}) (see Fig. S 9 in SI for specific capacity values). These results agree with those discussed in the previous section. Fig. 5c shows the charge/discharge profile of HC during test carried out at various current densities between 5 mV–2 V vs. Li^+/Li. As shown, the electrode displays the typical sloping charge/discharge profile of HC. It can be seen that the faradaic reaction involving binding of lithium ion at various sites (surface defects, graphitic interlayers, and closed pores) [27] of the hard carbon is initiated at potentials below 1.5 V vs Li^+/Li. A reversible specific capacity of 280 mA h g^{-1} is shown by the electrode at 1 C (372 mA g^{-1}). As expected, due to the different storage mechanism and a low diffusion of lithium-ion within the material, the capacity retention of the electrode at high current densities is lower than that of AC. Nonetheless, as shown in Fig. 5d, the electrode is able to display a specific capacity of more than 110 mA h g^{-1} at 10 C. This latter value is certainly promising for an HC tested in these conditions.

A LIC containing these two electrodes and having a mass ratio of 1:1 (HC//AC) was subsequently realized. The device was cycled between 2 V–4.3 V, while operating potential ranges for negative and positive electrode were accordingly fixed (more information available in SI 10). Fig. 5e shows a complete charge/discharge cycling profile of LIC in between 2 V–4.3 V vs. Li^+/Li at 1 A g^{-1}. The device displayed a specific capacity (referred to the mass of both electrodes) of 41 mAh g^{-1} and, it was able to retain 72% of its initial capacity after 8000 cycles carried out at 2 V–4.3 V vs. Li^+/Li at 1 A g^{-1} (Fig. 5f). This stability is comparable with that of several high performance devices reported in literature [23, 43–47]. Considering that this device can be further improved e.g., with a different electrode balancing, this result is certainly promising.

Fig. 6a is comparing the energy and power densities of the EDLC and the LIC investigated in this work. As shown, both devices display promising energy and power capabilities. The EDLC shows an energy density equivalent to 45 Wh kg_{AM}^{-1} and maintains its initial value by 65% even at very high current rate of 20 A g^{-1} signifying a high-power capability (28.6 kW kg_{AM}^{-1}). In the LIC, an obvious yield is a gain in energy density (138 Wh kg_{AM}^{-1}) which is more than triple the value obtained for EDLCs at given current density of 0.5 A g^{-1}. However, at higher current rates of 5 A g^{-1}, the power of the device decreases substantially. Such loss of energy at high power can certainly be mitigated to some extend by proper mass balancing. Nevertheless, the LIC is able to maintain high energy output of 152 – 34Wh kg_{AM}^{-1} at power densities of 312 W kg_{AM}^{-1}–12 kW kg_{AM}^{-1} which are highly comparable among the best biomass derived dual-carbon based LIC reported in literature [23, 43–47].

5. Conclusion

In this work we showed that the brewer's spent grains can be utilized to produce activated carbon with very high surface area and a large pore volume, and that is containing a large amount of meso and microporous structures. Composite electrodes containing this AC in organic electrolytes display very high capacitance and capacitance retention as well as good stability. These properties make a possible realization of a lab scale EDLCs and LICs displaying very high energy and power densities (45–29 Wh kg_{AM}^{-1} at power densities of 0.6–28.6 kW kg_{AM}^{-1} and 152–34 Wh kg_{AM}^{-1} at 0.3–12 kW kg_{AM}^{-1}, respectively). Taking these results into account, the AC derived from BSG can be certainly considered as very interesting materials, which can contribute to the development of high performance, cost effective and eco-friendly high-power devices.

CRediT authorship contribution statement

Sandesh Darlami Magar: Investigation, Writing – original draft, Supervision, Writing – review & editing. **Christian Leibing:** Investigation, Writing – original draft, Supervision, Writing – review & editing. **Juan Luis Gómez-Urbano:** Investigation, Writing – original draft, Supervision, Writing – review & editing. **Rosalía Cid:** Investigation, Writing – original draft, Supervision, Writing – review & editing. **Daniel Carriazo:** Supervision, Writing – review & editing. **Andrea Balducci:** Supervision, Writing – review & editing.

Declaration of Competing Interest

The authors declare no conflict of interest.

Data availability

Data will be made available on request.

Acknowledgments

S.D.M. C.L. and A.B. wish to thank the Deutsche Forschungsgemeinschaft (DFG) [project BA4956/21–1] and the Thüringer Ministerium für Wirtschaft, Wissenschaft und Digitale Gesellschaft (TMWWDG) and the Thüringer Aufbau Bank (TAB) within the project LiNaKon (2018 FGR 0092) for financial support. The authors wish to thank Lukas Köps in providing help for data management and data infrastructure, and the brewery "Jena Papiermühle" for providing spent grain sample.

Supplementary materials

Supplementary material associated with this article can be found, in the online version, at doi:10.1016/j.electacta.2023.142104.

References

[1] J.R. Miller, A.F. Burke, Electrochemical capacitors: challenges and opportunities for real-world applications, Electrochem. Soc. Interface 17 (2008) 53–57, https://doi.org/10.1149/2.f08081if.
[2] A.F. Burke, J. Zhao, Past, present and future of electrochemical capacitors: technologies, performance and applications, J. Energy Storage 35 (2021), 102310, https://doi.org/10.1016/j.est.2021.102310.
[3] T.P. Sumangala, M.S. Sreekanth, A. Rahaman, K.K. Kar, Applications of supercapacitors. Handbook of Nanocomposite Supercapacitor Materials, Ed., Springer International Publishing, Cham, 2021, pp. 367–393, https://doi.org/10.1007/978-3-030-68364-1_11. III Sel.
[4] Z. Lei, N. Christov, L.L. Zhang, X.S. Zhao, Mesoporous carbon nanospheres with an excellent electrocapacitive performance, J. Mater. Chem. 21 (2011) 2274–2281, https://doi.org/10.1039/c0jm03322g.
[5] B. Kim, H. Chung, W. Kim, High-performance supercapacitors based on vertically aligned carbon nanotubes and nonaqueous electrolytes, Nanotechnology 23 (2012), 155401, https://doi.org/10.1088/0957-4484/23/15/155401.
[6] A. Borenstien, M. Noked, S. Okashy, D. Aurbach, Composite carbon nano-tubes (CNT)/activated carbon electrodes for non-aqueous super capacitors using organic electrolyte solutions, J. Electrochem. Soc. 160 (2013) A1282–A1285, https://doi.org/10.1149/2.103308jes.
[7] D. Mhamane, A. Suryawanshi, A. Banerjee, V. Aravindan, S. Ogale, M. Srinivasan, Non-aqueous energy storage devices using graphene nanosheets synthesized by green route, AIP Adv. 3 (2013), 042112, https://doi.org/10.1063/1.4802243.
[8] W.W. Liu, X. Bin Yan, J.W. Lang, J. Bin Pu, Q.J. Xue, Supercapacitors based on graphene nanosheets using different non-aqueous electrolytes, New J. Chem. 37 (2013) 2186–2195, https://doi.org/10.1039/c3nj00335c.
[9] A. Krause, P. Kossyrev, M. Oljaca, S. Passerini, M. Winter, A. Balducci, Electrochemical double layer capacitor and lithium-ion capacitor based on carbon black, J. Power Sources 196 (2011) 8836–8842, https://doi.org/10.1016/j.jpowsour.2011.06.019.
[10] V. Barranco, M.A. Lillo-Rodenas, A. Linares-Solano, A. Oya, F. Pico, J. Ibañfez, F. Agullo-Rueda, J.M. Amarilla, J.M. Rojo, Amorphous carbon nanofibers and their activated carbon nanofibers as supercapacitor electrodes, J. Phys. Chem. C 114 (2010) 10302–10307, https://doi.org/10.1021/jp1021278.
[11] A. Laheäär, A.L. Peikolainen, M. Koel, A. Jänes, E. Lust, Comparison of carbon aerogel and carbide-derived carbon as electrode materials for non-aqueous supercapacitors with high performance, J. Solid State Electrochem. 16 (2012) 2717–2722, https://doi.org/10.1007/s10008-012-1660-4.
[12] Y. Korenblit, M. Rose, E. Kockrick, L. Borchardt, A. Kvit, S. Kaskel, G. Yushin, High-rate electrochemical capacitors based on ordered mesoporous silicon carbide-derived carbon, ACS Nano 4 (2010) 1337–1344, https://doi.org/10.1021/nn901825y.
[13] Z. Yue, H. Dunya, M. Ashuri, K. Kucuk, S. Aryal, S. Antonov, B. Alabbad, C. U. Segre, B.K. Mandal, Synthesis of a very high specific surface area active carbon and its electrical double-layer capacitor properties in organic electrolytes, ChemEngineering 4 (2020) 1–15, https://doi.org/10.3390/chemengineering4030043.
[14] W. Zhang, R.R. Cheng, H.H. Bi, Y.H. Lu, L.B. Ma, X.J. He, A review of porous carbons produced by template methods for supercapacitor applications, New Carbon Mater. 36 (2021) 69–81, https://doi.org/10.1016/S1872-5805(21)60005-7.
[15] J. Bates, F. Markoulidis, C. Lekakou, G.M. Laudone, Design of porous carbons for supercapacitor applications for different organic solvent-electrolytes, C. 7 (2021), 15, https://doi.org/10.3390/c7010015.
[16] E. Raymundo-Piñero, K. Kierzek, J. Machnikowski, F. Béguin, Relationship between the nanoporous texture of activated carbons and their capacitance properties in different electrolytes, Carbon 44 (2006) 2498–2507, https://doi.org/10.1016/j.carbon.2006.05.022. N. Y.
[17] J. Chmiola, G. Yushin, R. Dash, Y. Gogotsi, Effect of pore size and surface area of carbide derived carbons on specific capacitance, J. Power Sources 158 (2006) 765–772, https://doi.org/10.1016/j.jpowsour.2005.09.008.
[18] M. Karthik, E. Redondo, E. Goikolea, V. Roddatis, S. Doppiu, R. Mysyk, Effect of mesopore ordering in otherwise similar micro/mesoporous carbons on the high-rate performance of electric double-layer capacitors, J. Phys. Chem. C 118 (2014) 27715–27720, https://doi.org/10.1021/jp508581x.
[19] L. Jiang, L. Sheng, Z. Fan, Biomass-derived carbon materials with structural diversities and their applications in energy storage, Sci. China Mater. 61 (2018) 133–158, https://doi.org/10.1007/s40843-017-9169-4.
[20] B. Escobar, D.C. Martínez-Casillas, K.Y. Pérez-Salcedo, D. Rosas, L. Morales, S. J. Liao, L.L. Huang, X. Shi, Research progress on biomass-derived carbon electrode materials for electrochemical energy storage and conversion technologies, Int. J. Hydrog. Energy 46 (2021) 26053–26073, https://doi.org/10.1016/j.ijhydene.2021.02.017.
[21] Y. Gao, L. Li, Y. Jin, Y. Wang, C. Yuan, Y. Wei, G. Chen, J. Ge, H. Lu, Porous carbon made from rice husk as electrode material for electrochemical double layer capacitor, Appl. Energy 153 (2015) 41–47, https://doi.org/10.1016/j.apenergy.2014.12.070.
[22] D. Gandla, X. Wu, F. Zhang, C. Wu, D.Q. Tan, High-performance and high-voltage supercapacitors based on N-doped mesoporous activated carbon derived from dragon fruit peels, ACS Omega 6 (2021) 7615–7625, https://doi.org/10.1021/acsomega.0c06171.
[23] J.L. Gómez-Urbano, G. Moreno-Fernández, M. Arnaiz, J. Ajuria, T. Rojo, D. Carriazo, Graphene-coffee waste derived carbon composites as electrodes for optimized lithium ion capacitors, Carbon 162 (2020) 273–282, https://doi.org/10.1016/j.carbon.2020.02.052. N. Y.
[24] C. Poochai, A. Srikhaow, J. Lohitkarn, T. Kongthong, S. Tuantranont, S. Tuantranont, V. Primpray, N. Maeboonruan, A. Wisitsoraat, C. Sriprachuabwong, Waste coffee grounds derived nanoporous carbon incorporated with carbon nanotubes composites for electrochemical double-layer capacitors in organic electrolyte, J. Energy Storage 43 (2021), 103169, https://doi.org/10.1016/j.est.2021.103169.
[25] V. Ureña-Torres, G. Moreno-Fernández, J.L. Gómez-Urbano, M. Granados-Moreno, D. Carriazo, Graphene-wine waste derived carbon composites for advanced supercapacitors, ChemEngineering 6 (2022), https://doi.org/10.3390/chemengineering6040049.
[26] C.M. Ashraf, K.M. Anilkumar, B. Jinisha, M. Manoj, V.S. Pradeep, S. Jayalekshmi, Acid Washed, steam activated, coconut shell derived carbon for high power supercapacitor applications, J. Electrochem. Soc. 165 (2018) A900–A909, https://doi.org/10.1149/2.0491805jes.
[27] S.D. Magar, C. Leibing, J.L. Gómez-Urbano, D. Carriazo, A. Balducci, Brewers' Spent Grains-Derived Carbon as Anode for Alkali Metal-Ion Batteries, Energy Technol. 10 (2022), 2200379, https://doi.org/10.1002/ente.202200379.
[28] Eurostat, Happy International Beer Day!, Eurostat, 2019. https://ec.europa.eu/eurostat/en/web/products-eurostat-news/-/edn-20200807-1.
[29] K. Jagiełło, W. Hińcz, W. Kaczorowska, M. Jackowski, M. Bartman, J. Kaczmarczyk, Properties of activated carbon obtained from brewers spent grains, Biomass Convers. Biorefinery. (2022), https://doi.org/10.1007/s13399-022-02964-6.
[30] A.I. Osman, E. O'Connor, G. McSpadden, J.K. Abu-Dahrieh, C. Farrell, A.H. Al-Muhtaseb, J. Harrison, D.W. Rooney, Upcycling brewer's spent grain waste into activated carbon and carbon nanotubes for energy and other applications via two-stage activation, J. Chem. Technol. Biotechnol. 95 (2020) 183–195, https://doi.org/10.1002/jctb.6220.
[31] S. Doniach, M. Sunjic, Many-electron singularity in X-ray photoemission and X-ray line spectra from metals, J. Phys. C Solid State Phys. 3 (1970) 285–291, https://doi.org/10.1088/0022-3719/3/2/010.
[32] D. Wang, G. Fang, T. Xue, J. Ma, G. Geng, A melt route for the synthesis of activated carbon derived from carton box for high performance symmetric supercapacitor applications, J. Power Sources 307 (2016) 401–409, https://doi.org/10.1016/j.jpowsour.2016.01.009.
[33] D. Wang, S. Liu, G. Fang, G. Geng, J. Ma, From trash to treasure: direct transformation of onion husks into three-dimensional interconnected porous

carbon frameworks for high-performance supercapacitors in organic electrolyte, Electrochim. Acta 216 (2016) 405–411, https://doi.org/10.1016/j.electacta.2016.09.053.
[34] D. Lozano-Castelló, M.A. Lillo-Ródenas, D. Cazorla-Amorós, A. Linares-Solano, Preparation of activated carbons from Spanish anthracite - I. activation by KOH, Carbon 39 (2001) 741–749, https://doi.org/10.1016/S0008-6223(00)00185-8. N. Y.
[35] S. Li, K. Han, J. Li, M. Li, C. Lu, Preparation and characterization of super activated carbon produced from gulfweed by KOH activation, Microporous Mesoporous Mater. 243 (2017) 291–300, https://doi.org/10.1016/j.micromeso.2017.02.052.
[36] A. Kovtun, D. Jones, S. Dell'Elce, E. Treossi, A. Liscio, V. Palermo, Accurate chemical analysis of oxygenated graphene-based materials using X-ray photoelectron spectroscopy, Carbon 143 (2019) 268–275, https://doi.org/10.1016/j.carbon.2018.11.012. N. Y.
[37] D.J. Morgan, Comments on the XPS analysis of carbon materials, C. 7 (2021), 51, https://doi.org/10.3390/c7030051.
[38] G. Beamson, D.R. Briggs. High Resolution XPS of Organic Polymers: The Scienta ESCA300 Database, Wiley & Sons, Chichester, UK, 1992.
[39] A. Ferrari, J. Robertson, Interpretation of raman spectra of disordered and amorphous carbon, Phys. Rev. B Condens. Matter Mater. Phys. 61 (2000) 14095–14107, https://doi.org/10.1103/PhysRevB.61.14095.
[40] M. Zhu, C.J. Weber, Y. Yang, M. Konuma, U. Starke, K. Kern, A.M. Bittner, Chemical and electrochemical ageing of carbon materials used in supercapacitor electrodes, Carbon 46 (2008) 1829–1840, https://doi.org/10.1016/j.carbon.2008.07.025. N. Y.
[41] Y. Liu, B. Réty, C. Matei Ghimbeu, B. Soucaze-Guillous, P.L. Taberna, P. Simon, Understanding ageing mechanisms of porous carbons in non-aqueous electrolytes for supercapacitors applications, J. Power Sources 434 (2019), https://doi.org/10.1016/j.jpowsour.2019.226734.
[42] P. Azaïs, L. Duclaux, P. Florian, D. Massiot, M.A. Lillo-Rodenas, A. Linares-Solano, J.-.P. Peres, C. Jehoulet, F. Béguin, Causes of supercapacitors ageing in organic electrolyte, J. Power Sources 171 (2007) 1046–1053, https://doi.org/10.1016/j.jpowsour.2007.07.001.
[43] S. Li, P. Liu, X. Zheng, M. Wu, High-performance dual carbon lithium-ion capacitors based on nitrogen-doped 2D carbon nanosheets as both anode and cathode, Electrochim. Acta 428 (2022), 140921, https://doi.org/10.1016/j.electacta.2022.140921.
[44] P. Sennu, N. Arun, S. Madhavi, V. Aravindan, Y.S. Lee, All carbon based high energy lithium-ion capacitors from biomass: the role of crystallinity, J. Power Sources 414 (2019) 96–102, https://doi.org/10.1016/j.jpowsour.2018.12.089.
[45] D. Sui, M. Wu, Y. Liu, Y. Yang, H. Zhang, Y. Ma, L. Zhang, Y. Chen, High performance Li-ion capacitor fabricated with dual graphene-based materials, Nanotechnology 32 (2020) 15403, https://doi.org/10.1088/1361-6528/abb9d8.
[46] M. Zhang, X. Zheng, J. Mu, P. Liu, W. Yuan, S. Li, X. Wang, H. Fang, H. Liu, T. Xing, H. Hu, M. Wu, Robust and fast lithium storage enabled by polypyrrole-coated nitrogen and phosphorus Co-doped hollow carbon nanospheres for lithium-ion capacitors, Front. Chem. 9 (2021) 1–10, https://doi.org/10.3389/fchem.2021.760473.
[47] H. Chao, J. Liu, Preparation of the 3D Porous Carbon Based on Vacuum residue and Its Application in Lithium Ion Capacitors, J. Phys. Conf. Ser. 2044 (2021) 12117, https://doi.org/10.1088/1742-6596/2044/1/012117.